



This is a repository copy of *Comparative performance study of alternate fault-tolerant inverter configurations for direct torque control-based three-phase PM BLAC drives under single-phase open-circuit fault.*

White Rose Research Online URL for this paper:

<https://eprints.whiterose.ac.uk/99726/>

Version: Accepted Version

Proceedings Paper:

Hoang, K. orcid.org/0000-0001-7463-9681 and Zhu, Z.Q. (2016) Comparative performance study of alternate fault-tolerant inverter configurations for direct torque control-based three-phase PM BLAC drives under single-phase open-circuit fault. In: 8th IET International Conference on Power Electronics, Machines and Drives (PEMD 2016). IET international conference on Power Electronics, Machines and Drives, 19-21 Apr 2016, Glasgow, UK. IET . ISBN 978-1-78561-188-9

<https://doi.org/10.1049/cp.2016.0193>

This paper is a postprint of a paper submitted to and accepted for publication in 8th IET International Conference on Power Electronics, Machines and Drives (PEMD 2016) and is subject to Institution of Engineering and Technology Copyright. The copy of record is available at IET Digital Library

Reuse

Items deposited in White Rose Research Online are protected by copyright, with all rights reserved unless indicated otherwise. They may be downloaded and/or printed for private study, or other acts as permitted by national copyright laws. The publisher or other rights holders may allow further reproduction and re-use of the full text version. This is indicated by the licence information on the White Rose Research Online record for the item.

Takedown

If you consider content in White Rose Research Online to be in breach of UK law, please notify us by emailing eprints@whiterose.ac.uk including the URL of the record and the reason for the withdrawal request.



eprints@whiterose.ac.uk
<https://eprints.whiterose.ac.uk/>

Comparative performance study of alternate fault-tolerant inverter configurations for direct torque control-based three-phase PM BLAC drives under single-phase open-circuit fault

K. D. Hoang and Z.Q. Zhu

Department of Electronic and Electrical Engineering, The University of Sheffield, Mappin Street, S1 3JD, United Kingdom

Keywords: Direct torque control, fault-tolerant inverter configurations, permanent magnet (PM) brushless AC (BLAC) machine, single-phase open-circuit fault (SOF).

Abstract

This paper presents a comparative performance study of three typical fault-tolerant control (FTC) topologies [split-capacitor (SC), extra-leg split-capacitor (ELSC), and extra-leg extra-switch (ELES)] for direct torque control (DTC)-based three-phase permanent magnet (PM) brushless AC (BLAC) drives under single-phase open-circuit fault (SOF). The advantages and limitations of these FTC schemes are theoretically compared and empirically validated. To achieve reliable post-fault operations, control issues associated with VM-based flux estimators employed for DTC-based BLAC drives under SOF are demonstrated and relevant remedies are proposed. It is shown that although the ELES scheme can maintain the normal based speed, 6 of its 8 switching states cause phase-to-neutral short circuit in one or both two remaining phase windings resulting in high current harmonic values. Besides, during its implementation, the full DC-link voltage value is always applied to the non-short circuit phase windings leading to high possibility of winding insulation damage. Thus, for a compromise of the normal based speed by a factor of $\sqrt{3}/2$, the ELSC drive should be used to avoid these issues. Furthermore, in the low-speed region up to half of the rated speed, the lowest copper loss, current harmonics, and torque ripples can be obtained by utilizing the SC drive.

1 Introduction

Due to its high efficiency and wide flux-weakening capability, permanent magnet (PM) brushless AC (BLAC) machine is widely employed in many industrial applications which demand high performance operation [1]-[2]. In some safety-critical systems such as aerospace or automotive industry, a fault-tolerant drive with its capability of providing reliable post-fault operation is essentially required [3]. In literature, the fault-tolerant control (FTC) topic is very large [4]-[7]. Because of its highest percentage of registered failures in practice, faulty events within the power inverter resulting in single-phase open-circuit faults (SOF) is the main scope of this paper [8], [9]. Based on the post-fault reconfigurations [10], FTC topologies for three-phase BLAC drive under SOF can be categorized into three schemes: split-

capacitor (SC) drive, Fig. 1(a), extra-leg split-capacitor (ELSC) drive, Fig. 1(b), and extra-leg extra-switch (ELES) drive, Fig. 1(c). In the SC scheme, the electromagnetic torque in the post-fault case is still contributed by three stator phase currents [11]. Therefore, demanded current for a given torque is similar for both the healthy and the post-fault cases, Fig. 1(d). However, magnitude of the voltage vector applied to the machine terminals decreases to half of its pre-fault value [11]. As a result, the based speed of the SC drive reduces one-half of its pre-fault rated value.

Besides, for the ELSC and the ELES drives to achieve a similar demanded torque as that in the pre-fault case, an increase in magnitude by a factor of $\sqrt{3}$ together with a 60 electrical-degree phase shift must be maintained for the two remaining phase currents [10], Fig. 1(d). In practice, the post-fault operation with current magnitude as 1.732 times of the pre-fault rated value may result in magnetic saturation issue leading to maximum achievable torque reduction. Ideally, for a demanded torque, copper loss in the ELSC and ELES topologies are 2 times higher than the SC scheme. On the other hand, value of the voltage applied to each remaining phase winding of the ELSC drive always varies between $-V_{dc}/2$ and $+V_{dc}/2$ [3]. Hence, based speed of the ELSC drive is reduced by a factor $\sqrt{3}/2$ of its rated value. Furthermore, under the ELES scheme, similar voltage vector magnitude as the pre-fault case can be achieved [12]. Hence, the normal based speed can be retained in its post-fault operating mode.

The performances of three FTC schemes in Fig. 1 applied to a hysteresis current control (HCC)-based BLAC drive were studied and reported in [10] where it was shown that high-performance operation in the post-fault mode can be achieved by appropriately modifying the HCC methodology. Applications of direct torque control (DTC) technique to a SC-based and ELES-based BLAC drives were respectively reported in [11] and [12] where novel current model (CM)-based flux estimators together with novel voltage model (VM)-based flux estimators considering unbalanced inverter voltage drops (IVDs) were proposed and empirically verified. In this paper, an expansion of the previous works is presented via a comparative performance study of three typical FTC schemes for DTC-based BLAC drives in terms of current harmonics, torque ripples, maximum applied voltage, and achievable based speed. To avoid parameter mismatches and saturation effects, VM-based flux estimators proposed in [11], [12] are utilized. For reliable post-fault operation achievements, the relative effects of the unbalanced IVD, the

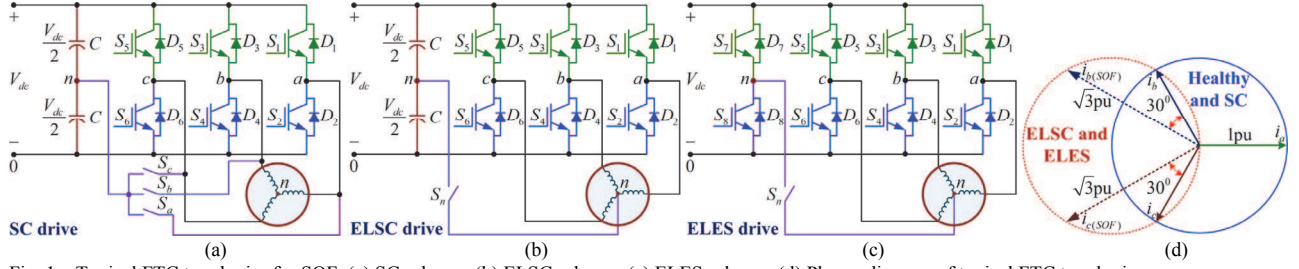


Fig. 1. Typical FTC topologies for SOF. (a) SC scheme. (b) ELSC scheme. (c) ELES scheme. (d) Phasor diagram of typical FTC topologies.

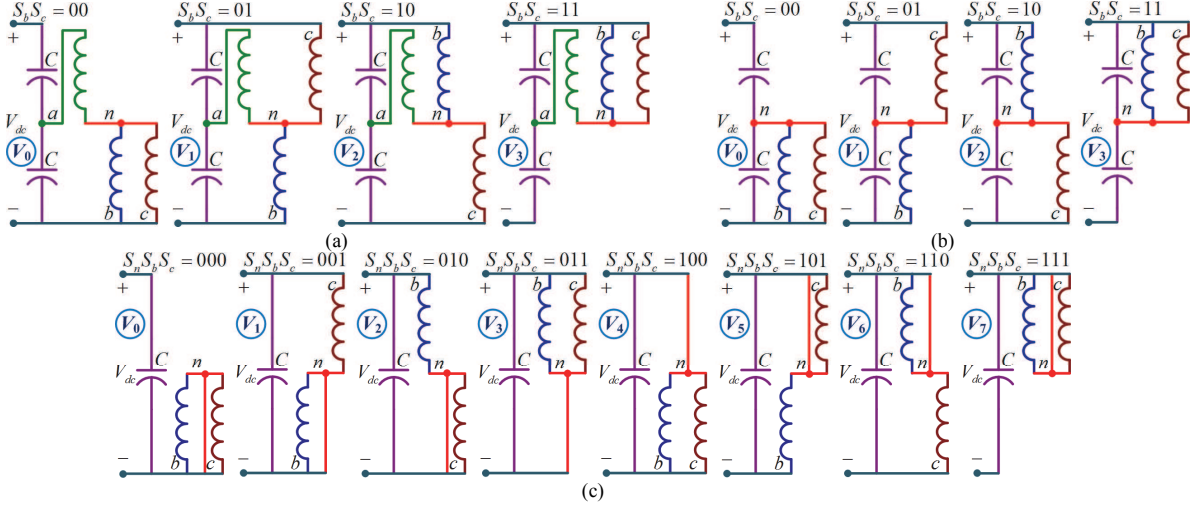


Fig. 2. Switching states of typical FTC topologies. (a) SC scheme. (b) ELSC scheme. (c) ELES scheme.

midpoint voltage variation of the DC link capacitor bank, and the measurement disturbances on the employed VM-based flux estimators together with their remedies are empirically demonstrated. It is shown that although the ELES drive can maintain the normal based speed, 6 of its 8 switching states cause phase-to-neutral short circuit in one or both the two remaining phase windings resulting in high current harmonic values. In addition, during its implementation, there is a high possibility of winding insulation damage as the full DC-link voltage value is always applied to the non-short circuit phase windings. To avoid these issues, the ELSC drive can be employed with a compromise of the normal based speed by a factor of $\sqrt{3}/2$. In the low-speed region up to the half rated speed, the SC drive should be utilized with lowest copper loss, current harmonics, and torque ripples compared with the other two schemes.

2 DTC techniques for BLAC drives under SOF

2.1 Mathematical model of PM BLAC machine under SOF

Assuming phase a is the open-phase, the mathematical model for PM BLAC machine under both healthy and SOF [11], [12] in the $(\alpha\beta)$ reference frame is represented as follows

$$v_\alpha = R_s i_\alpha / k_F + d\psi_{s\alpha} / dt; \quad v_\beta = R_s i_\beta / k_F + d\psi_{s\beta} / dt \quad (1)$$

$$\psi_{s\alpha} = L_s i_\alpha / k_F + \psi_m \cos(\theta_e); \quad \psi_{s\beta} = L_s i_\beta / k_F + \psi_m \sin(\theta_e) \quad (2)$$

$$T_e = 3p(\psi_{s\alpha} i_\beta - \psi_{s\beta} i_\alpha) / 2 / k_F \quad (3)$$

where $i_{\alpha,\beta}$, $v_{\alpha,\beta}$, $\psi_{s\alpha,\beta}$ are respectively the transformed $(\alpha\beta)$ currents, voltages, and stator fluxes; L_s is the stator

inductance; R_s is the stator resistance; T_e is the electromagnetic torque; ψ_m is the PM flux linkage; θ_e is the electrical rotor position; and p is the pole-pair number. For the ELSC and ELES schemes, the $(\alpha\beta)$ current components in (1)-(3) is derived by modifying the conventional Clarke transformation [10], [12]. The factor $k_F = 1$ for the healthy and SC drives and $k_F = \sqrt{3}$ for the ELSC and ELES schemes. The magnitude and angular position of the stator flux vector, ψ_s and θ_{ψ_s} , are given by

$$\psi_s = \sqrt{\psi_{s\alpha}^2 + \psi_{s\beta}^2}; \quad \theta_{\psi_s} = \arctan(\psi_{s\beta} / \psi_{s\alpha}) \quad (4)$$

2.2 Lookup table (LUT)-based DTC techniques for BLAC drives under SOF

Under LUT-based DTC technique, both the stator flux magnitude and electromagnetic torque are simultaneously controlled via a predefined optimum switching look-up table (LUT) [11], [12]. Based on the assumption that the open phase is phase a , the available switching states for the SC, ELSC, and ELES schemes are respectively presented in Figs. 2(a), 2(b), and 2(c). As can be seen, there are 4 available switching states for the SC and the ELSC schemes and 8 available switching states for the ELES scheme. Although the voltage vectors associated with similar switching states for both the SC and the ELSC schemes situate at similar positions in the $(\alpha\beta)$ plane, Fig. 3(a), implementation of each switching state results in different phase-to-neutral voltage values applied to phase windings, Figs. 2(a) and 2(b). For the SC drive, the feasible voltages applied to each phase windings is: $\pm V_{dc}/3$ and 0 for the non-active phase (phase a) and $\pm V_{dc}/6$ and $\pm V_{dc}/2$ for the active phase (phase b and c) [11]. It is

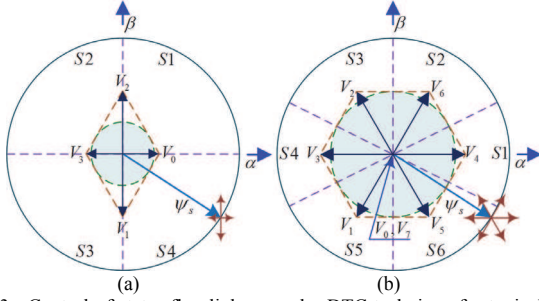


Fig. 3. Control of stator flux linkage under DTC technique for typical FTC topologies. (a) SC and ELSC schemes. (b) Healthy and ELES schemes.

Table 1: Optimum switching table of DTC-based SC and DTC-based ELSC schemes

$d\psi_s$	dT_e	Sector			
		S1	S2	S3	S4
1	1	V_2	V_3	V_1	V_0
	0	V_0	V_2	V_3	V_1
0	1	V_3	V_1	V_0	V_2
	0	V_1	V_0	V_2	V_3

Table 2: Optimum switching table of DTC-based healthy and ELES schemes

$d\psi_s$	dT_e	Sector					
		S1	S2	S3	S4	S5	S6
1	1	V_6	V_2	V_3	V_1	V_5	V_4
	0	V_7	V_0	V_7	V_0	V_7	V_0
	-1	V_5	V_4	V_6	V_2	V_3	V_1
0	1	V_2	V_3	V_1	V_5	V_4	V_6
	0	V_0	V_7	V_0	V_7	V_0	V_7
	-1	V_1	V_5	V_4	V_6	V_2	V_3

noted that the feasible voltages applied to each phase winding of the healthy case is: $\pm V_{dc}/3$, $\pm 2V_{dc}/3$, and 0. Thus, magnitude of the voltage vector applied to the SC drive reduces to one-half of the healthy case [11]. Hence, achievable based speed of the SC drive reduces to a half of its pre-fault value. On the other hand, Fig. 2(b) shows that the feasible voltages applied to the two remaining phase windings under the ELSC scheme always varies between $-V_{dc}/2$ and $+V_{dc}/2$. Compared with the pre-fault case where the voltage vector magnitude under the well-known space vector modulation technique is $V_{dc}/\sqrt{3}$, the based speed of the ELSC drive is reduced by a factor of $\sqrt{3}/2$. Furthermore, due to its similar achievable voltage vector magnitude as the pre-fault mode, Fig. 3(b), the ELES scheme can maintain the same based speed as the healthy case [12]. However, implementation of its switching states (excepting V_3 and V_4) results in short circuit in one or both two remaining phase windings, Fig. 2(c). In addition, in comparison with the pre-fault, the SC, and the ELSC cases, under the ELES scheme, the highest feasible voltage value ($\pm V_{dc}$) is applied to the non-short circuit phase windings. Thus, extremely high current harmonics and torque ripples may be obtained for the ELES drive [10], [12]. Besides, the possibility of winding insulation damage is inevitable for the two remaining phase windings [the authors experienced turn-to-ground short circuit on one remaining phase winding during testing the ELES drive-see Fig. 8(c)].

By dividing the stator flux ($\alpha\beta$) plane under the SC and the ELSC schemes into 4 equal sectors spaced 90 electrical degrees, Fig. 3(a), and the stator flux ($\alpha\beta$) plane under the

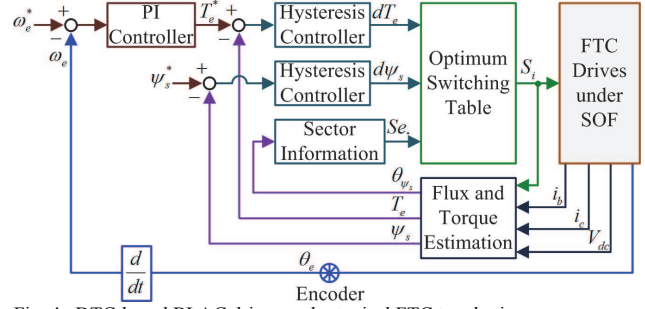


Fig. 4. DTC-based BLAC drives under typical FTC topologies.

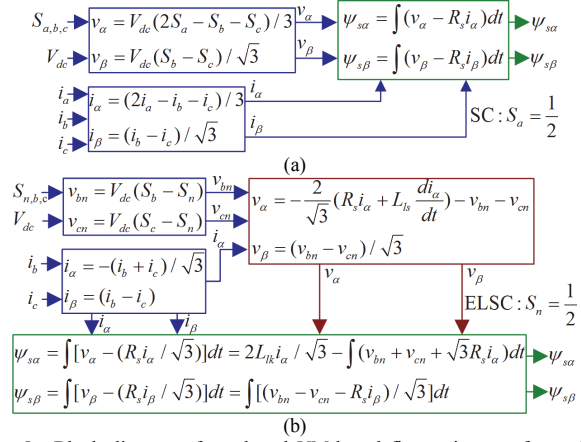


Fig. 5. Block diagram of employed VM-based flux estimators for typical FTC topologies. (a) SC and ELSC schemes. (b) Healthy and ELES schemes.

ELES scheme into 6 equal sectors spaced 60 electrical degrees (similar to the healthy case), Fig. 3(b), the optimum switching table for both the DTC-based SC and DTC-based ELSC schemes [11], and the DTC-based healthy and ELES schemes [12] is respectively illustrated in Tables 1 and 2 where $d\psi_s$ and dT_e is respectively the output of the stator flux magnitude and the electromagnetic hysteresis controllers, Fig. 4. Obviously, control quality of DTC-based drives highly depends on the accurateness of the employed stator flux estimators which can be categorized into two main models: the current model (CM) relying on the stator inductance, the PM flux linkage, and the rotor position information as shown in (2); and the voltage model (VM) depending on the machine resistance, the stator leakage inductance L_{lk} (only the ELSC and the ELES schemes), and the integration step as presented in (1) [11], [12]. It is noted that for the ELSC and the ELES schemes to achieve the pre-fault rated torque, the increase by a factor of $\sqrt{3}$ for the two remaining phase currents may result in parameter mismatches and saturation issues. Thus, performance of the CM-based flux estimators under these FTC schemes may become degraded. To achieve a fair performance evaluation for three typical FTC topologies in Fig. 1, the VM-based flux estimators [11], [12], which is not affected by these parameter mismatches and saturation issues, is selected, Fig. 5. After the stator flux ($\alpha\beta$) components have been estimated, the relevant electromagnetic torque together with the magnitude and angular position of the stator flux vector in Fig. 4 can be computed via (3) and (4), respectively.

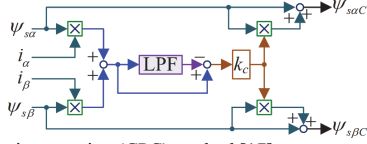


Fig. 6. Centre point correction (CPC) method [17].

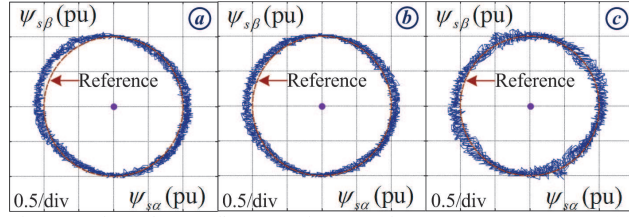


Fig. 7. Estimated stator flux (pu) of ELSC scheme at 750rpm, 0.15Nm. (a) Without compensation. (b) Incorporating IVD compensation method. (c) Incorporating IVD compensation and CPC methods.

3 Control issues of VM-based DTC BLAC drives under SOF and relevant remedies

3.1 Imbalanced inverter voltage drop (IVD)

In [11] and [12], it is proven that the reconfiguration from the typical six-switch three-phase topology in the pre-fault case into the SC or the ELES schemes may result in an imbalance between the inverter voltage drop (IVD) ($\alpha\beta$) components. This unbalanced issue does make the predicted stator flux components obtained from the VM-based flux estimators shown in Fig. 5 becomes unbalanced in magnitude. As a result, the current waveforms of VM-based DTC BLAC drives under the SC or the ELES schemes become seriously distorted [11], [12]. Similar phenomenon can be deduced for the VM-based DTC ELSC scheme. By considering the IVDs of one inverter leg as a forward voltage drop, V_F , connected in series with an on-state resistance voltage drop, $R_{ON}i$, compensation for IVD effects on the VM-based flux estimators can be obtained by introducing relevant IVD corrective values in the voltage equations (1) as follows.

$$v_{\alpha IVD} = R_{ON}i_\alpha + [2\text{sgn}(i_\alpha) - \text{sgn}(i_b) - \text{sgn}(i_c)]V_F / 3 \quad (5)$$

$$v_{\beta IVD} = R_{ON}i_\beta + [\text{sgn}(i_b) - \text{sgn}(i_c)]V_F / \sqrt{3} \quad (6)$$

IVD corrective values for the SC scheme [11]

$$v_{\alpha IVD} = -R_{ON}i_\alpha / 3 - [\text{sgn}(i_b) + \text{sgn}(i_c)]V_F / 3 \quad (7)$$

$$v_{\beta IVD} = R_{ON}i_\beta + [\text{sgn}(i_b) - \text{sgn}(i_c)]V_F / \sqrt{3} \quad (8)$$

IVD corrective values for the ELSC scheme

$$v_{\alpha IVD} = R_{ON}i_\alpha / \sqrt{3} - [\text{sgn}(i_b) + \text{sgn}(i_c)]V_F \quad (9)$$

$$v_{\beta IVD} = R_{ON}i_\beta / \sqrt{3} + [\text{sgn}(i_b) - \text{sgn}(i_c)]V_F / \sqrt{3} \quad (10)$$

IVD corrective values for the ELES scheme [12]

$$v_{\alpha IVD} = 3\sqrt{3}R_{ON}i_\alpha - [\text{sgn}(i_b) + \text{sgn}(i_c) + 2\text{sgn}(i_n)]V_F \quad (11)$$

$$v_{\beta IVD} = R_{ON}i_\beta / \sqrt{3} + [\text{sgn}(i_b) - \text{sgn}(i_c)]V_F / \sqrt{3} \quad (12)$$

3.2 Midpoint DC link voltage variation and current measurement disturbances

Theoretically, the two capacitors of the DC link capacitor bank in the SC and ELSC drives [Figs. 1(a) and 1(b)] are often considered as identical and ideal and therefore, the midpoint voltage in the relevant VM-based flux estimators

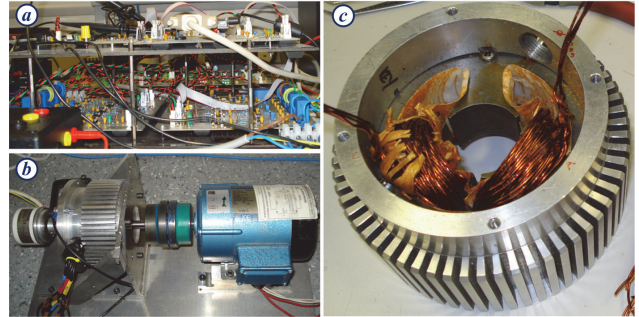


Fig. 8. Experimental hardware setup. (a) Inverter and DSP control platform. (b) PM BLAC machine coupled to brushed DC generator. (c) PM BLAC machine with turn-to-ground short circuit issue during testing ELES scheme.

Table 3: Parameters of tested PM BLAC machine

Phase resistance / Dq-axis inductance	0.466 Ω / 3.19 mH
PM flux-linkage / Number of pole pairs	92.8 mWb / 1
DC bus voltage / Rated current	70 V / 2.2 A
Rated speed / Rated torque	3000 rpm / 0.3 Nm

respectively shown in Figs. 5(a) and 5(b) is often assumed as constant ($V_{dc}/2$). In practice, these two capacitors are often non-identical with different equivalent series inductances and resistances [13]. Thus, variation of the midpoint voltage value is inevitable. Also in Fig. 5(b), the estimated flux α -component is partly contributed by measurements of phase currents which do not involve in the integration step. Hence, although the pure integrator is typically replaced by a low-pass filter (LPF) [12], DC offset, noise, or measurement disturbances inherently existing in current sensors will inevitably express in the predicted flux α -component. Thus, for the VM-based flux estimators in Fig. 5, eccentric predicted stator flux linkage may be obtained. In DTC-based BLAC drives, the stator flux linkage is often regulated to be an origin-centred circular path in the steady-state [11], [12]. Hence, this eccentric estimated stator flux issue resulting in significantly distorted current waveforms may lead to the FTC drive system instabilities. Among the FTC topologies Fig. 1, the performance of the ELSC scheme may be mostly affected by this eccentric estimated stator flux issue due to the contributions of the midpoint voltage assumed as constant ($V_{dc}/2$) together with the measured phase currents on its employed VM-based flux estimator, Fig. 5(b).

Up to date, a number of strategies were suggested to mitigate the LPF negative effects [14]-[16] and thus, improving the performance of VM-based flux estimators. However, these LPF negative effects do not contribute to the aforementioned eccentric estimated stator flux issue. In [17], it was demonstrated that the scalar product of the estimated stator flux components and the sensed phase currents can be used to form a centre point correction (CPC) method for the estimated stator flux in DTC-based drive systems, Fig. 6. Similar method is adopted to mitigate the influences of the eccentric estimated flux issue for the employed VM-based flux estimators in Fig. 5. Measurements of estimated stator flux linkage under the VM-based DTC ELSC scheme at low-speed operation (750rpm) and half rated torque (0.15Nm) without and incorporating the relevant compensation methods are illustrated in Fig. 7. As can be seen in Fig. 7(a), without considering the proposed compensation methods, a seriously

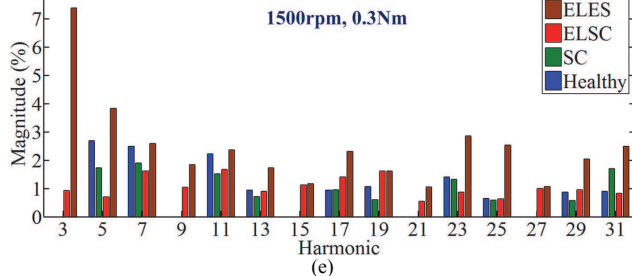
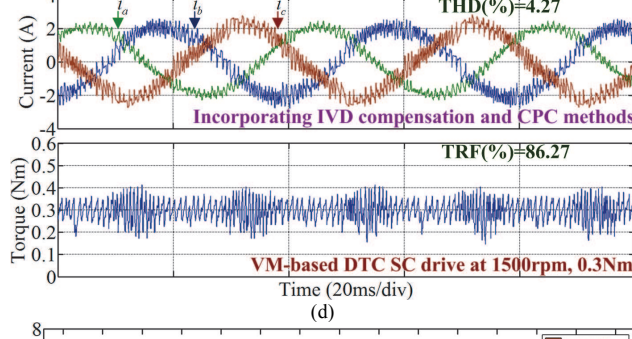
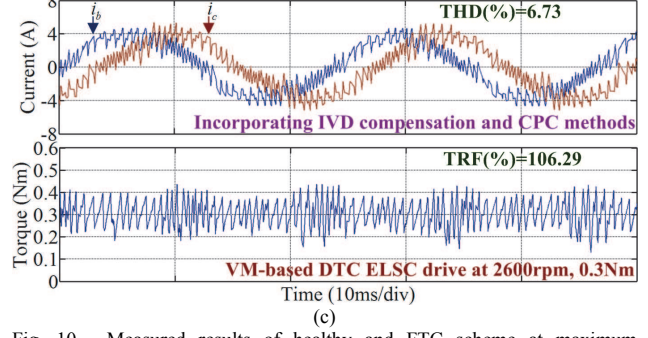
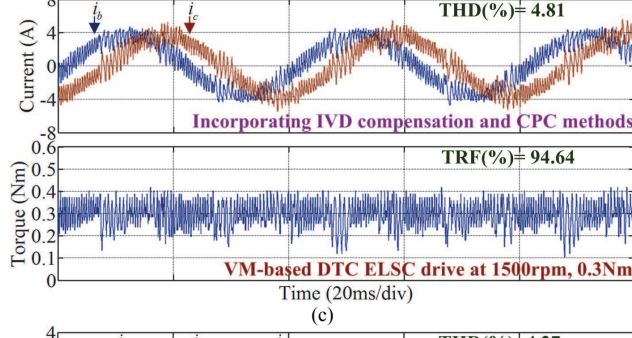
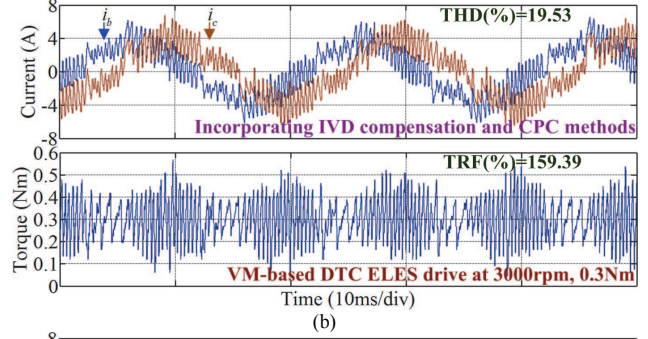
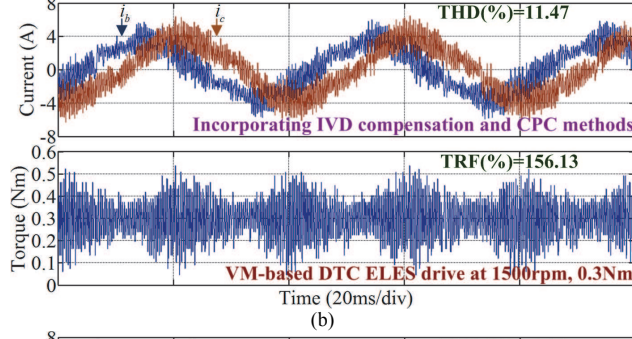
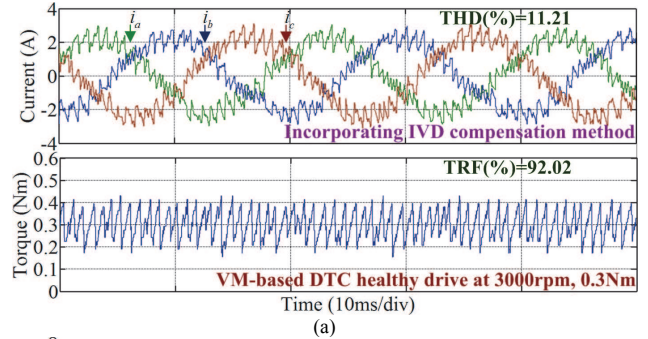
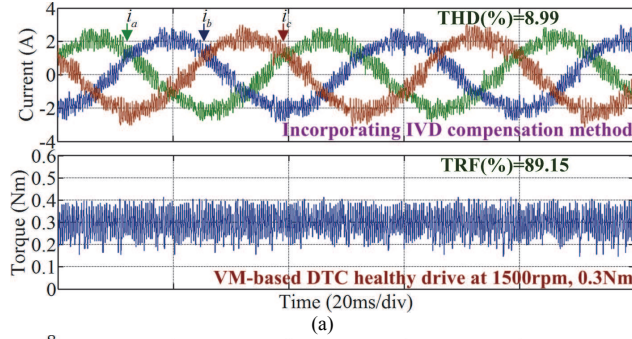


Fig. 9. Measured results of healthy and FTC schemes at 1500rpm, 0.3Nm. (a) Healthy case. (b) ELES scheme. (c) ELSC scheme. (d) SC scheme. (e) Current harmonic values in (%) of fundamental component.

Fig. 10. Measured results of healthy and FTC scheme at maximum achievable based speed, 0.3Nm. (a) Healthy case at 3000rpm. (b) ELES scheme at 3000rpm. (c) ELSC scheme at 2600rpm.

VM-based flux estimator, Fig. 5(b). Although this eccentric issue can be considerably mitigated using the relevant IVD compensation method in (9) and (10), the predicted stator flux linkage is still not fully followed the circular reference locus, Fig. 7(b). By incorporating both the IVD compensation and the CPC methods, a better estimated flux linkage compared with Fig. 7(b) can be achieved with the predicted flux linkage is well regulated around its circular reference locus, Fig. 7(c).

4 Experimental results

The performances of three studied VM-based DTC FTC topologies with the healthy case acting as a benchmark were evaluated by measurements on a BLAC drive with neutral connection, [11] and [12], Fig. 8. Under the SC and ELSC schemes, both $d\psi_s$ and dT_e in Table 1 are set as zero. For the healthy and the ELES schemes (Table 2) to exploit the merits of zero voltage vectors, $d\psi_s$ is set as zero and dT_e is chosen as 2% of the rated torque. The flux reference is set to peak value of the PM flux-linkage. The employed machine parameters and ratings are provided in Table 3. The inverter is realized by an intelligent power module (International Rectifier

IRAMY20UP60B) of which V_F and R_{ON} are 0.9V and 0.075 Ω , respectively. The current total harmonic distortion (THD) and torque ripple factor (TRF) were defined in [10]. Measurements of the tested VM-based DTC BLAC drive in the pre-fault case and the post-fault cases with the three studied FTC topologies at half rated speed (1500rpm) are presented in Fig. 9. As discussed above, employment of the SC scheme results in the lowest feasible voltage applied to the phase windings. Thus, under the rated-load torque (0.3Nm), lowest current THD and TRF values are obtained for the tested SC-based BLAC drive, Fig. 9(d). On the other hand, under the ELES scheme, due to the highest voltage (V_{dc}) applied to the phase windings together with its short-circuit issue, highest current THD and TRF values are observed in Fig. 9(b). Furthermore, compared with the healthy case, Fig. 9(a), a lower current THD value and nearly similar TRF value (94.64% compared with 89.15%) can be attained for the ELSC scheme, Fig. 9(c). The current harmonics under different FTC topologies compared with the pre-fault case are depicted in Fig. 9(e). As can be seen, due to the neutral connection, employment of the ELSC or the ELES schemes provides a path for the third-order current harmonics. However, due to the aforementioned short-circuit and full applied DC link voltage issues, highest values of low-order current harmonics are derived for the ELES scheme. As the SC drive can only be operated up to half of the normal rated speed [11], measurements of the ELES and the ELSC drives at their maximum achievable based speed are presented in Figs. 10(b) and 10(c), respectively. It is noted that implementations of these schemes with current magnitude as 1.732 times of the pre-fault rated value may lead to the possibility of maximum achievable torque reduction due to the saturation effects. By comparing Fig. 10(b) with Fig. 10(a), it is shown that the ELES drive can maintain the normal rated speed (3000rpm) with increase in copper loss (2 times), current THD value (1.74 times), and TRF value (1.73 times). Fig. 11(c) demonstrates that for a lower achievable based speed (2600rpm), the ELSC drive can be employed with significantly lower current THD and TRF values.

5 Conclusions

In this paper, a comparative performance study of three typical FTC topologies for VM-based DTC BLAC drives under SOF in terms of current harmonics, torque ripple, applied voltage, and achievable based speed has been presented. For reliable post-fault operating achievements, control issues associated with the employed VM-based flux estimators have been demonstrated together with relevant compensation methods. It has been shown that although the ELES drive can maintain the pre-fault based speed, 6 of its 8 switching states cause phase-to-neutral short circuit in one or both two remaining phase windings. In addition, under the ELES scheme, there is a high possibility of winding insulation damage because the voltage value applied to the non-short circuit phase windings is always the full DC-link voltage. The combination of these issues cause highest current THD and TRF values for the ELES scheme. Thus, for a reduction of the normal based speed by a factor of $\sqrt{3}/2$,

the ELSC drive should be used with lower current THD and TRF values to avoid these issues. Furthermore, although the SC drive can only maintain half of the pre-fault based speed, implementation of this scheme results in lowest copper loss, current THD and TRF values.

References

- [1] K. D. Hoang and K. Atallah, "A rapid concept development technique for electric vehicle power trains," in *Proc. IEEE Int. Conf. Connected Vehicles and Export (ICCVE) 2014*, Vienna, Austria, Nov. 3-7, 2014, pp. 191-198.
- [2] B. A. Hoang and H. K. A. Aorith, "Online control of IPMSM drives for traction applications considering machine parameter and inverter nonlinearities," *IEEE Trans. Transp. Electrification*, vol. 1, no. 4, pp. 312-325, Dec. 2015.
- [3] B. A. Hoang, T. A. Lipo, T. M. Jahns, and S. E. Schulz, "Fault tolerant three-phase AC motor drive topologies: a comparison of features, cost, and limitations" *IEEE Trans. Power Electron.*, vol. 19, no. 4, pp. 1108-1116, Jul. 2004.
- [4] S. Nandi, H. A. Toliyat, and X. Li, "Condition monitoring and fault diagnosis of electrical motors-A review," *IEEE Trans. Energy Convers.*, vol. 20, no. 4, pp. 719-729, Dec. 2005.
- [5] B. Lu and S. K. Sharma, "A literature review of IGBT fault diagnostic and protection methods for power inverters," *IEEE Trans. Ind. Appl.*, vol. 45, no. 5, pp. 1770-1777, Sep./Oct. 2009.
- [6] W. Zhang, D. Xu, P. N. Enjeti, H. Li, J. T. Hawke, and H. S. Krishnamoorthy, "Survey on fault-tolerant techniques for power electronic converters," *IEEE Trans. Power Electron.*, vol. 29, no. 12, pp. 6319-6331, Dec. 2014.
- [7] G. F. H. Beng, X. Zhang, and D. M. Vilathgamuwa, "Sensor fault-resilient control of interior permanent-magnet synchronous motor drives," *IEEE/ASME Trans. Mechatronics*, vol. 20, no. 2, pp. 855-864, Apr. 2015.
- [8] G. R. Catuogno, G. O. Garcia, and R. Leidhold, "Fault-tolerant inverter for power flow control in variable-speed four-wire permanent-magnet generators," *IEEE Trans. Ind. Electron.*, vol. 62, no. 11, pp. 6727-6736, Nov. 2015.
- [9] A. Kontarcek, P. Bajec, M. Nemecek, V. Ambrozic, and D. Nedeljkovic, "Cost-effective three-phase PMSM drive tolerant to open-phase fault," *IEEE Trans. Ind. Electron.*, vol. 62, no. 11, pp. 6708-6718, Nov. 2015.
- [10] K. D. Hoang, Z. Q. Zhu, M. P. Foster, and D. A. Stone, "Comparative study of current vector control performance of alternate fault tolerant inverter topologies for three-phase PM brushless AC machine with one phase open-circuit fault," in *Proc. IET Int. Conf. Power Electron. Mach. Drives*, Brighton, UK, April 19-21, 2010, pp. 1-6.
- [11] K. D. Hoang, Z. Q. Zhu, and M. P. Foster, "Influence and compensation of inverter voltage drop in direct torque controlled four-switch three-phase PM brushless AC drives," *IEEE Trans. Power Electron.*, vol. 26, no. 8, pp. 2343-2357, Aug. 2011.
- [12] K. D. Hoang, Z. Q. Zhu, and M. P. Foster, "Direct torque control of permanent magnet brushless AC drive with single-phase open-circuit fault accounting for influence of inverter voltage drop," *IET Electric Power Applications*, vol. 7, no. 5, pp. 369-380, May 2013.
- [13] H. Wang and F. Blaabjerg, "Reliability for DC-link applications in power electronic converter-an overview," *IEEE Trans. Ind. Appl.*, vol. 50, no. 5, pp. 3569-3578, Sep./Oct. 2014.
- [14] J. Hu and B. Wu, "New integration algorithms for estimating motor flux over a wide speed range," *IEEE Trans. Power Electron.*, vol. 13, no. 5, pp. 969-977, Sep. 1998.
- [15] M. F. Rahman, Md. E. Haque, L. Tang, and L. Zhong, "Problems associated with the direct torque control of an interior permanent-magnet synchronous motor drive and their remedies," *IEEE Trans. Ind. Electron.*, vol. 51, no. 4, pp. 799-809, Aug. 2004.
- [16] D. Stojic, M. Milinkovic, S. Veinovic, and I. Klasnic, "Improved stator flux estimator for speed sensorless induction motor drives," *IEEE Trans. Power Electron.*, vol. 30, no. 4, pp. 2363-2371, Apr. 2015.
- [17] J. Luukko, M. Niemela, and J. Pyrhonen, "Estimation of flux linkage in a direct-torque-controlled drive," *IEEE Trans. Ind. Electron.*, vol. 50, no. 2, pp. 283-287, Apr. 2003.